Advanced numerical simulation of magnetic liquid sloshing in microgravity

Á. Romero-Calvo[1], M.A. Herrada[2], G. Cano-Gómez[3], H. Schaub[4]

The term sloshing refers to the movement of liquids in partially filled containers. Low-gravity sloshing plays an important role in the configuration of space vehicles, as it affects their dynamics and complicates the propellant management system design. Magnetic forces can be used to position a susceptible fluid, tune its natural frequencies, and increase its damping ratios in low-gravity. However, prior work shows that the analysis of this phenomenon, named magnetic liquid sloshing, requires advanced modeling capabilities. This paper introduces a coupled magnetohydrodynamic (MHD) model for the study of low-gravity axisymmetric magnetic liquid oscillations. The incompressible, viscous mass and momentum balances are solved together with the steady-state Maxwell equations by following a monolithic solution scheme. The method is fully implicit, allowing to reach a steady-state solution in a single time step. Five regions are used to discretize the simulation domain, that combines non-singular mappings and a meshfree approach. The steady-state solution (basic flow) is verified with equivalent computations from Comsol Multiphysics assuming the geometry and physical properties of the ESA Drop Your Thesis! 2017 drop tower experiment. Future steps include the study of linear oscillations, free surface stability properties, and lateral oscillations, among others.

1 Introduction

Propellant sloshing represents a major concern for space engineers due to its impact on the dynamics of space vehicles. During launch, the uncontrolled movement of liquids may lead to a total or partial mission failure [1]. In microgravity, sloshing becomes highly stochastic, resulting in a complicated propellant management and attitude control system design [2]. Propellant Management Devices (PMD) are commonly employed to ensure a gas-free expulsion of propellant, fix the center of mass of the liquid, and increase its sloshing frequencies and damping ratios. However, they also increase the inert mass of the vehicle and complicate numerical analysis [3, 4].

A gravity-equivalent force may be generated by means of electromagnetic fields as an alternative to classical PMDs and active settling methods. The use of *dielectrophoresis*, a phenomenon on which an electric force is exerted on dielectric materials, was explored by the US Air Force with suitable propellants in 1963. The study unveils a high risk of arcing inside the tanks and highlights the need for large, heavy and noisy power sources [5]. The magnetic equivalent, named *Magnetic Positive Positioning* (MP^2), has also been suggested to exploit the inherent properties of paramagnetic, diamagnetic, and ferromagnetic liquids [6–8].

MP^2 devices must deal with the rapid decay of magnetic fields with distance, that limits their reachability to relatively small regions. This difficulty may be compensated by employing highly susceptible liquids, such as ferrofluids. Ferrofluids are colloidal suspensions of magnetic nanoparticles developed in the early 1960s to enhance the controllability of rocket propellants [7]. Despite having numerous applications on Earth, contributions addressing their original purpose are still scarce. Normal-gravity works have explored fundamental aspects of the dynamics of magnetic liquids, such as the natural frequency shifts due to the magnetic interac-

tion [9], axisymmetric sloshing [10, 11], two-layer sloshing [12], liquid swirling [13] or the development of tuned magnetic liquid dampers [14, 15]. Low-gravity contributions include the gravity compensation experiments performed by Dodge in 1972, that indirectly addressed the low-gravity sloshing of ferrofluids subjected to quasi-uniform magnetic forces [16]. Motivated by the advent of stronger permanent magnets and high-temperature superconductors, the NASA MAPO experiment validated the magnetic positioning of liquid oxygen in a series of parabolic flights in 2001 [6]. Subsequent works present refined numerical models and results of technical relevance [17–25]. The axisymmetric sloshing of water-based ferrofluids was characterized in microgravity when subjected to an inhomogeneous magnetic field as part of the ESA Drop Your Thesis! 2017 campaign [26–29]. As a follow-up, the lateral sloshing of ferrofluids was studied in the framework of the UNOOSA DropTES Programme 2019 [30, 31].

Most existing works assume that the fluid-magnetic problem described by the MP^2 concept can be studied with a set of uncoupled fluid-magnetic equations [6, 16–25]. This is appropriate for low-susceptibility fluids, such as liquid oxygen or liquid hydrogen. The development of coupled magnetohydrodynamic simulation frameworks has however been identified as a key step towards the design of novel magnetic liquid sloshing devices [8]. Since the position of a highly-susceptible fluid modifies the magnetic field distribution, such numerical models should simultaneously solve the Navier-Stokes (fluid-dynamic) and Maxwell (magnetic) equations. Desired results include, but are not limited to, sloshing modes and frequencies, free surface stability properties, viscous damping coefficients, and time-dependent simulations.

This ongoing project describes the implementation of the capillary fluid modeling methodology developed by Herrada and Montanero [32] and includes the magnetostatic Maxwell equations and associated fluid-magnetic interactions to study the axisymmetric magnetic sloshing problem. Unlike the quasi-analytical coupled magnetic sloshing model developed by the authors in Ref. 33, the fluid-magnetic equations are solved simultaneously (not iteratively) and a viscous fluid is assumed. The numerical method is described in Sec. 3, and the verification of the steady-state solution is performed in Sec. 4. Section 5 summarizes the main conclusions and

---

[1]Department of Aerospace Engineering Sciences, University of Colorado Boulder, CO, United States; `alvaro.romerocalvo@colorado.edu`

[2]Departamento de Ingeniería Aeroespacial y Mecánica de Fluidos, Universidad de Sevilla, Sevilla, Spain; `herrada@us.es`

[3]Departamento de Física Aplicada III, Universidad de Sevilla, Sevilla, Spain; `gabriel@us.es`

[4]Department of Aerospace Engineering Sciences, University of Colorado Boulder, CO, United States; `hanspeter.schaub@colorado.edu`
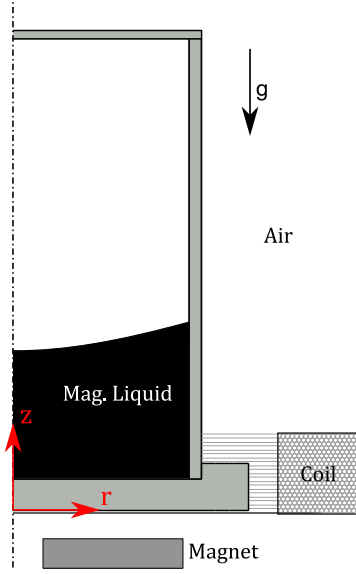
Fig. 1: Problem formulation

future steps of the work.

2 Problem formulation

The system under analysis, represented in Fig. 1, consists on a partially filled cylindrical tank subjected to the influence of a coil or magnet. The vessel has radius R, height h, and holds a volume V of an incompressible, Newtonian, magnetic liquid with density ρ, specific volume $\nu = \rho^{-1}$, shear coefficient of viscosity η, and surface tension σ. The static contact angle between the liquid and the wall is θ_c. A non-reactive inviscid gas at pressure p_g fills the free space. The system is subjected to an inertial acceleration g along the vertical axis and to an inhomogeneous, axisymmetric magnetic field imposed by either a coil or a magnet.

The magnetohydrodynamic model here developed is designed to provide the axisymmetric (i) meniscus profile, (ii) free surface oscillation frequencies, (iii) free surface stability properties, and (iv) time evolution of the system. Although the model can be applied to different tank geometries, liquids, and magnetic configurations, the experimental setup implemented for the ESA Drop Your Thesis! 2017 experiment [26–28] has been chosen to conduct the verification of results. Such experiment studies the axisymmetric free surface oscillations frequencies of a ferrofluid solution subject to an inhomogeneous magnetic field in microgravity, and is hence appropriate for the validation of the numerical model presented in this manuscript.

2.1 Stress tensor and force distributions

The magnetodynamic state of an incompressible continuous medium can be described by means of the viscous Maxwell stress tensor, given by [34–37]

$$\mathcal{T} = \mathcal{T}_p + \mathcal{T}_\nu + \mathcal{T}_m, \tag{1}$$

where the pressure, viscous, and magnetic terms are

$$\mathcal{T}_p = -p^* \, \boldsymbol{I}, \tag{2a}$$

$$\mathcal{T}_\nu = \eta \left[\nabla \boldsymbol{v} + (\nabla \boldsymbol{v})^T \right], \tag{2b}$$

$$\mathcal{T}_m = -\frac{\mu_0}{2} H^2 \boldsymbol{I} + \boldsymbol{B}\boldsymbol{H}, \tag{2c}$$

and where

$$p^* = p(\nu, T) + \mu_0 \int_0^H \frac{\partial}{\partial \nu} \left[\nu M \right] dH' \tag{3}$$

is the *composite pressure* including the hydrostatic $p(\nu, T)$ and magnetopolarization terms. In these expressions, $\boldsymbol{B} = \mu_0 \left(\boldsymbol{H} + \boldsymbol{M} \right)$, $\boldsymbol{H}$, and $\boldsymbol{M}$ are the flux density, magnetic, and magnetization fields, μ_0 is the permeability of vacuum, $\boldsymbol{I} = \delta_{ij} \boldsymbol{e}_i \boldsymbol{e}_j$ is the unit dyadic in the Cartessian $\boldsymbol{e}_i$ reference system, and $\boldsymbol{v}$ is the fluid velocity. For soft magnetic materials, the magnetization field is aligned with the magnetic field and follows the relation $\boldsymbol{M} = \chi^{\text{vol}}(H)\boldsymbol{H}$, with $\chi^{\text{vol}}(H)$ being the volume magnetic susceptibility. Applications involving unequilibrated ferrofluid solutions, for which $\boldsymbol{M} \times \boldsymbol{H} \neq 0$, should incorporate the effects resulting from particle rotation. An additional term must be added to the viscous stress tensor T_ν, and the angular momentum and magnetic relaxation equations also have to be considered [36, 37].

The forces per unit volume exerted on the medium in the absence of electric fields can be computed as the divergence of the stress tensor given by Eq. 1, resulting in [37]

$$\boldsymbol{f} = \boldsymbol{f}_p + \boldsymbol{f}_\nu + \boldsymbol{f}_m, \tag{4}$$

with

$$\boldsymbol{f}_p = \nabla \cdot \mathcal{T}_p = -\nabla p^*, \tag{5a}$$

$$\boldsymbol{f}_\nu = \nabla \cdot \mathrm{T}_\nu = \nabla \cdot \left\{ \eta \left[\nabla \boldsymbol{v} + (\nabla \boldsymbol{v})^T \right] \right\}, \tag{5b}$$

$$\boldsymbol{f}_m = \nabla \cdot \mathcal{T}_m = \mu_0 M \nabla H = \mu_0 (\boldsymbol{M} \cdot \nabla) \boldsymbol{H} \tag{5c}$$

If the viscosity coefficient η is constant, the viscous term reduces to

$$\boldsymbol{f}_\nu = \eta \nabla^2 \boldsymbol{v}. \tag{6}$$

However, ferrofluids exhibit a nonlinear dependence of the shear coefficient of viscosity η with H through [38, 39]

$$\frac{\Delta \eta}{\zeta} = \frac{\mu_0 M_0 H \tau}{4\zeta + \mu_0 M_0 H \tau} \sin^2 \beta, \tag{7}$$

where ζ is the *vortex viscosity*, τ is the *Brownian relaxation time*, M_0 is the unperturbed magnetization value, and β is the angle between the magnetic field $\boldsymbol{H}$ and the vorticity vector Ω. For dilute ferrofluids, $\zeta = (3/2)\eta\phi$, with ϕ being the volume fraction of solids in the ferrofluid [38]. This effect is negligible for most applications, but may be relevant for concentrated ferrofluids subjected to strong magnetic fields.

Surface forces appear in the gas-liquid interface as a consequence of the discontinuity in the stress tensor. Those forces are balanced according to the *ferrohydrodynamic incompressible viscous boundary condition*. Assuming a contact between a ferrofluid and a non-magnetic, inviscid gas, the condition is expressed in normal (n) and tangential (t) components as [37]

$$n: \quad p^* - 2\eta \frac{\delta v_n}{\delta x_n} + p_n - p_0 = 2\sigma \mathcal{H}, \tag{8a}$$

$$t: \quad \eta \left(\frac{\partial v_n}{\partial x_t} + \frac{\partial v_t}{\partial x_n} \right) = 0, \tag{8b}$$

with $\boldsymbol{n}$ being the external normal vector, $p_n = \mu_0 M_n^2/2$ the *magnetic normal traction*, $\mathcal{H}$ the mean curvature of the interface, v_n and v_t the normal and tangential velocity components, and x_n and x_t the distances along the normal and tangential directions, respectively.

2.2 Governing equations for a magnetic, viscous, incompressible fluid

The magnetohydrodynamic mass and momentum conservation equations deriving from the stress tensor given by Eq. 1 are [37]

$$\nabla \cdot \boldsymbol{v} = 0, \tag{9a}$$

$$\rho \frac{D\boldsymbol{v}}{Dt} = \rho \boldsymbol{g} + \boldsymbol{f}_p + \boldsymbol{f}_\nu + \boldsymbol{f}_m, \tag{9b}$$

with D denoting the material derivative, and t the time. This system of equations is subjected to an appropriate set of boundary conditions. Particular attention should be payed to those described by Eq. 8 for magnetic systems.

The terms $\boldsymbol{f}_p$ and $\boldsymbol{f}_m$ are defined by the fields $\boldsymbol{H}$, $\boldsymbol{B}$, and $\boldsymbol{M}$, which have to be computed at each time step by solving the magnetic problem. Assuming a static magnetic configuration without surface currents and electric fields, the steady-state Maxwell's equations are given by

$$\nabla \cdot \boldsymbol{B} = 0, \tag{10a}$$

$$\nabla \times \boldsymbol{H} = \boldsymbol{J}_e, \tag{10b}$$

where $\boldsymbol{J}_e$ is the volume density of electric current. If no surface currents are applied to the system, the magnetic boundary conditions become

$$\boldsymbol{n} \cdot (\boldsymbol{B}_2 - \boldsymbol{B}_1) = 0, \tag{11a}$$

$$\boldsymbol{n} \times (\boldsymbol{H}_2 - \boldsymbol{H}_1) = 0, \tag{11b}$$

with $\boldsymbol{n}$ being the external normal vector. Therefore, the normal component of $\boldsymbol{B}$ and the tangential component of $\boldsymbol{H}$ are continuous across the interface.
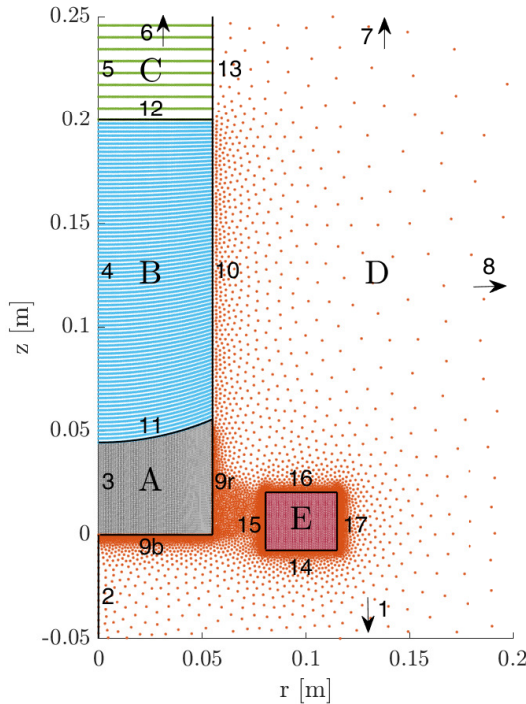

Fig. 2: Numerical simulation domain and labels for the mapped (A,B,C,E) and meshless (D) regions and interfaces. The external boundary of region D is a cylinder of 0.6 m radius and 1.2 m height.

3 Numerical method

The theoretical framework described in the previous section is here implemented adopting the cylindrical reference system $\{\boldsymbol{e}_r, \boldsymbol{e}_\phi, \boldsymbol{e}_z\}$ shown in Fig. 1. The simulation domain is divided into five regions and their corresponding interfaces, as shown in Fig. 2: A (liquid domain), B (air domain inside the container), C (air domain over the container), D (surrounding air environment), and E (the coil or magnet domains).

3.1 Axisymmetric Navier-Stokes equations

The mass and momentum conservation equations defined by Eq. 9 should be expressed in the cylindrical reference system after considering the axisymmetry of the problem. This results in

$$\frac{\partial(ru)}{\partial r} + \frac{\partial(rw)}{\partial r} = 0, \tag{12a}$$

$$\rho \left(\frac{\partial u}{\partial t} + u \frac{\partial u}{\partial r} + w \frac{\partial u}{\partial z} \right) = -\frac{\partial p^*}{\partial r} +$$
$$\eta \left(\frac{\partial^2 u}{\partial r^2} + \frac{\partial(u/r)}{\partial r} + \frac{\partial^2 u}{\partial z^2} \right) + \mu_0 \left(M_r \frac{\partial H_r}{\partial r} + M_z \frac{\partial H_r}{\partial z} \right), \tag{12b}$$

$$\rho \left(\frac{\partial w}{\partial t} + u \frac{\partial w}{\partial r} + w \frac{\partial w}{\partial z} \right) = -\frac{\partial p^*}{\partial z} +$$
$$\eta \left(\frac{\partial^2 w}{\partial r^2} + \frac{1}{r} \frac{\partial w}{\partial r} + \frac{\partial^2 w}{\partial z^2} \right) + \mu_0 \left(M_r \frac{\partial H_z}{\partial r} + M_z \frac{\partial H_z}{\partial z} \right), \tag{12c}$$

where r (z) is the radial (axial) coordinate, and u (w) is the radial (axial) velocity component. The axisymmetry of the magnetic problem has been taken into account in the previous expressions, so that $\boldsymbol{J}_e$ has only azimuthal components, and $\boldsymbol{M}$ and $\boldsymbol{H}$ lack from them, resulting in $\boldsymbol{H} = H_r \boldsymbol{e}_r + H_z \boldsymbol{e}_z$, and $\boldsymbol{M} = M_r \boldsymbol{e}_r + M_z \boldsymbol{e}_z$. When a magnet is implemented, its magnetization only consists on a vertical component, so the axisymmetry properties are maintained.

3.2 Magnetic potentials formulation

Equations (10a) and (10b) can be rewritten as a function of $\boldsymbol{H}$, resulting in

$$\nabla \cdot \boldsymbol{H} = -\nabla \cdot \boldsymbol{M}, \tag{13a}$$

$$\nabla \times \boldsymbol{H} = \boldsymbol{J}_e. \tag{13b}$$

Therefore, $\boldsymbol{H}$ has scalar sources in the magnetized region and vector sources in the coil. According to Helmholtz's theorem, $\boldsymbol{H}$ can be expressed in terms of scalar and vector magnetic potentials. Taking into account the axisymmetry of the problem,

$$H_r = -\frac{1}{r} \frac{\partial \Psi}{\partial z} - \frac{\partial \Phi}{\partial r}; \quad H_z = \frac{1}{r} \frac{\partial \Psi}{\partial r} - \frac{\partial \Phi}{\partial z}, \tag{14}$$

where Φ is the scalar potential generated by scalar sources, and the stream-like function $\Psi = r A_e(r, z)/\mu_0$ is directly related to the azimuthal component $A_e(r, z)$ of the vector magnetic potential created by the electric current. The magnetic problem is then formulated and solved in terms of Φ and Ψ by noting that

$$\nabla \cdot \boldsymbol{H} = -\left[\frac{\partial^2 \Phi}{\partial z^2} + \frac{\partial^2 \Phi}{\partial r^2} + \frac{1}{r} \frac{\partial \Phi}{\partial r} \right], \tag{15}$$

$$\nabla \times \boldsymbol{H} = -\frac{1}{r} \left[\frac{\partial^2 \Psi}{\partial r^2} + \frac{\partial^2 \Psi}{\partial z^2} - \frac{1}{r} \frac{\partial \Psi}{\partial r} \right] \boldsymbol{u}_\phi. \tag{16}$$

In the domain A, $\boldsymbol{M} = \chi^{\text{vol}}(H)\boldsymbol{H}$ and Eq. (13a) becomes

$$\frac{\partial^2 \Phi}{\partial z^2} + \frac{\partial^2 \Phi}{\partial r^2} + \frac{1}{r}\frac{\partial \Phi}{\partial r} = \frac{1}{1 + \chi^{\text{vol}}(H)} \left(H_r \frac{\partial \chi^{\text{vol}}}{\partial r} + H_z \frac{\partial \chi^{\text{vol}}}{\partial z} \right), \tag{17}$$

where χ^{vol} also depends on Ψ and Φ through the magnetization law

$$\chi^{\text{vol}} = a_M \frac{\arctan(c_M H)}{H} + b_M \frac{\arctan(d_M H)}{H} + e_M. \tag{18}$$

For domains B-E, Eq. (13a) is simply $\nabla \cdot \boldsymbol{H} = 0$ due to the absence of inhomogeneous magnetization fields (since the magnet is uniformly magnetized). When the domain $\boldsymbol{E}$ is occupied by a coil,

$$\boldsymbol{J}_e = \frac{NI}{S_c} \boldsymbol{e}_\phi, \tag{19}$$

with N being the number of wire turns, I the current flowing through each of them, and S_c the cross section of the coil. Consequently, Eq. (13b) adopts the form

$$-\frac{1}{r} \left[\frac{\partial^2 \Psi}{\partial r^2} + \frac{\partial^2 \Psi}{\partial z^2} - \frac{1}{r}\frac{\partial \Psi}{\partial r} \right] = \frac{NI}{S_c}. \tag{20}$$

For domains A-D (and E, when it represents a magnet), $\boldsymbol{J}_e = 0$, and the previous expression simplifies to $\nabla \times \boldsymbol{H} = \boldsymbol{0}$. If a magnet with uniform, vertical magnetization field occupies the region E, the condition $\boldsymbol{M} = M_m \boldsymbol{u}_z$ is imposed and the stream-like function has the trivial solution $\Psi = 0$.

3.3 Boundary conditions

An axisymmetric boundary condition is applied at the axis of symmetry for both fluid and magnetic problems, while the wall-liquid interaction is described by the non-penetration boundary condition. This results in

$$3: \quad u = 0, \quad \frac{\partial w}{\partial r} = 0, \tag{21}$$

$$9b: \quad u = w = 0, \tag{22}$$

$$9r: \quad u = w = 0. \tag{23}$$

In order to compute the viscous damping parameters of the problem, the mesh has to be refined at the walls 9b and 9r. The interfacial conditions described by Eq. 8 are particularized at the free fluid surface 11 by following a parametrization of the form $z_{\text{in}} = G(s,t)$ and $r_{\text{in}} = F(s,t)$, resulting in the normal balance

$$p^* + p_n - p_0 = \frac{\sigma}{F} \left(\frac{\partial F}{\partial s} \right)^{-1} \frac{\partial}{\partial s} \left[\frac{F \frac{\partial G}{\partial s}}{\sqrt{\left(\frac{\partial F}{\partial s}\right)^2 + \left(\frac{\partial G}{\partial s}\right)^2}} \right]$$
$$+ 2\eta \frac{\frac{\partial u}{\partial r}\left(\frac{\partial G}{\partial s}\right)^2 + \frac{\partial w}{\partial z}\left(\frac{\partial F}{\partial s}\right)^2 - \left(\frac{\partial w}{\partial r} + \frac{\partial u}{\partial z}\right)\frac{\partial F}{\partial s}\frac{\partial G}{\partial s}}{\left(\frac{\partial G}{\partial s}\right)^2 + \left(\frac{\partial F}{\partial s}\right)^2}, \tag{24a}$$

and the kinematic and geometric compatibility equations

$$\left(u - \frac{\partial F}{\partial t} \right) \frac{\partial G}{\partial s} - \left(w - \frac{\partial G}{\partial t} \right) \frac{\partial F}{\partial s} = 0, \tag{24b}$$

$$\frac{\partial G}{\partial s} \frac{\partial^2 G}{\partial s^2} + \frac{\partial F}{\partial s} \frac{\partial^2 F}{\partial s^2} = 0, \tag{24c}$$

where s is the arc length coordinate along the interface. The contact angle θ_c is imposed at the wall ($s = 1$) through

$$\frac{\partial F}{\partial s} \tan\left(\frac{\pi}{2} - \theta_c \right) + \frac{\partial G}{\partial s} = 0, \quad and \quad F = R. \tag{24d}$$

The magnetic boundary conditions derive from Eq. 11 after noting that the magnetic liquid and magnet are magnetized, while the coil has null magnetization. This results in

$$2 - 5: \quad H_r = 0, \quad B_r = 0, \tag{25}$$

$$9b, 9r, 11: \quad H_{t,1} = H_{t,2}, \quad B_{n,1} = B_{n,2}, \tag{26}$$

$$14 - 17 \, (coil): \quad \boldsymbol{H}_1 = \boldsymbol{H}_2, \quad \boldsymbol{B}_1 = \boldsymbol{B}_2, \tag{27}$$

$$14 - 17 \, (magnet): \quad H_{t,1} = H_{t,2}, \quad B_{n,1} = B_{n,2}, \tag{28}$$

$$10, 12, 13: \quad \boldsymbol{H}_1 = \boldsymbol{H}_2, \quad \boldsymbol{B}_1 = \boldsymbol{B}_2. \tag{29}$$

The potentials Ψ and Φ are truncated at the external contour (1,6-8) by considering the magnetic dipole term of the coil (c), and magnetized (m) domains, which are characterized by the moments $\boldsymbol{m}_\alpha = m_\alpha \boldsymbol{u}_z$ located at $\boldsymbol{r}_\alpha = z_\alpha \boldsymbol{u}_z$ (with $\alpha = c, m$). If the external contour is sufficiently separated from the magnetic sources, the potential vector of the system becomes similar to that of the dipole associated with the coil, and then

$$\Psi(r,z)|_{1,6-8} \approx \frac{m_c}{4\pi} \frac{r^2}{[r^2 + (z - z_c)^2]^{3/2}}. \tag{30}$$

The scalar potential Φ is generated by the magnetized media. Assuming that its contribution to the $\boldsymbol{H}$ field at the external contour is approximately equal to the contribution of the dipole terms of the magnet and magnetized liquid, the condition

$$(-\nabla\Phi)_{1,6-8} \approx \boldsymbol{H}_m^{\text{dip}} \tag{31}$$

is satisfied, and

$$\left(-\frac{\partial \Phi}{\partial r} \right)_{1,6-8} \approx \sum_i \frac{3m_{m,i}}{4\pi} \frac{r(z - z_{m,i})}{[r^2 + (z - z_{m,i})^2]^{5/2}} \bigg|_{1,6-8}, \tag{32a}$$

$$\left(-\frac{\partial \Phi}{\partial z} \right)_{1,6-8} \approx \sum_i \frac{m_{m,i}}{4\pi} \frac{2(z - z_{m,i})^2 - r^2}{[r^2 + (z - z_{m,i})^2]^{5/2}} \bigg|_{1,6-8}. \tag{32b}$$

Although the dipoles associated with the coil and magnet can be calculated beforehand, the dipole produced by the magnetized liquid needs to be approximated iteratively by integrating $\boldsymbol{M}$ in the domain A.

It should be noted that, if the system only includes magnets and magnetized liquids, the boundary condition given by Eq. (30) becomes unnecessary, since $\Psi(r,z) = 0$. Similarly, it is possible to impose $\Phi_{1,6-8} \approx 0$ when a weakly magnetized liquid and a coil are considered. Although less rigorous, the magnetic isolation condition $\Phi_{1,6-8} = \Psi_{1,6-8} = 0$ can also be imposed for very large simulation domains.

3.4 Solution procedure

The numerical procedure used in this study is a variation of that developed in Herrada & Montanero for interfacial flows [32]. As shown in Fig. 2, the simulation domain is divided into five blocks that implement different discretization methods.

Domains A, B and C is mapped onto a rectangular domain by means of non singular mappings

$$r_A = F(s,t), \quad z_A = G(s,t)\eta_A, \tag{33a}$$

$$r_B = F(s,t), \quad z_B = G(s,t) + [h - G(s,t)]\eta_B \quad \text{(33b)}$$

$$r_C = F(s,t), \quad z_C = H + [h_{\text{top}} - h]\eta_C, \quad \text{(33c)}$$

where h_{top} is the height of the domain, $0 \leq s \leq 1$, $0 \leq \eta_A \leq 1$, $0 \leq \eta_B \leq 1$, and $0 \leq \eta_C \leq 1$.

The derivatives appearing in the governing equations are expressed in terms of s, η, and t. Then, the resulting equations are discretized in the s direction using second-order finite differences with n_s equally spaced points. In the η direction, second-order finite differences are also employed with $n_{\eta A}$, $n_{\eta A}$, and $n_{\eta C}$ equally spaced points. This discretization strategy gives rise to meshes that automatically adapt to any variation of the free liquid interface ($r_{\text{in}} = F(s,t), z_{\text{in}} = G(s,t)$). The fixed domain E is discretized using second-order finite differences with n_{r_E} (n_{z_E}) equally spaced points in the radial (axial) direction. The results presented in this work are obtained using $n_s = 81$, $n_{\eta A} = 81$, $n_{\eta B} = 81$, $n_{\eta C} = 81$, $n_{r_E} = 51$, and $n_{z_E} = 51$.

In order to gain flexibility in the geometrical configuration of the external magnetic sources, a meshless method is followed to discretize the domain D. The boundary nodes in contact with domains A, B, C, and E are forced to have the same coordinates as those in the connecting domains. This implies that all points in contact with A and B move in accordance with the fluid. On the contrary, lines 1, 2, 7 and 8 have a fixed discretization. A 2D Matlab-based Delaunay mesh generator[5] is used to obtain the nodes of the grid with a maximum element size of 3 cm and a maximum growth rate of 0.1 [40]. The spatial derivatives in the D domain are computed from a set of 7 neighbors surrounding each node, which have the minimum virtual distance

$$d_v = \sqrt{(f^{k_r}\Delta r)^2 + (f^{k_z}\Delta z)^2}, \quad \text{(34)}$$

where $f \approx 0.25$ is a weighting factor, k_r (k_z) is a binary index that is set to 1 if the node belongs to a horizontal (vertical) boundary, becoming 0 otherwise, and $\{\Delta r, \Delta z\}$ are the relative cylindrical coordinates of the neighbors referred to the central node. This algorithm results in a good conditioning of the boundary nodes by promoting the selection a set of neighbors in the interior of the domain. Once the neighbors are defined, a second order Moving Least Squares algorithm [41] with six polynomial terms and a quartic weight function with a scale length of 10 cm is employed to compute the collocation matrices. Since the points in contact with A and B change for each time step, only a limited number of neighbors and collocation matrices is updated, resulting in an enhanced computational efficiency. The result of the discretization is represented in Fig. 2.

To compute the meniscus (steady-state solution), all the equations of the system are solved together (monolithic scheme) by employing a Newton–Raphson technique. In this work, second order backward differences are used to compute the time derivatives, and since the method is fully implicit, the time step is chosen to be sufficiently large to ensure that a steady state is reached in a single step. One of the main characteristics of this procedure is that the elements of the Jacobian matrix are obtained by combining analytical functions and the collocation matrices of all subdomains. This allows taking advantage of the sparsity of the resulting matrix to reduce the computational time on each Newton-Raphson iteration.

---

[5] https://github.com/dengwirda/mesh2d. Consulted on: 05/07/2020

4 Verification and validation

The magnetohydrodynamic model here introduced is an extension of the capillary model presented in Ref. 32, which has already been validated with experimental measurements at the International Space Station. After verifying that the fluid-dynamic results in the absence of magnetic fields are correct, the verification and validation process focuses on the magnetic modules. In this section, fundamental results are compared with analogous magnetostatic models and analytical predictions. The geometrical and physical configurations of the ESA Drop Your Thesis! 2017 experiment [29] is implemented.

The magnetic ($\boldsymbol{H}$) and magnetization ($\boldsymbol{M}$) fields are first compared in Figs. 3 and 4 with a geometrically equivalent solution from Comsol Multiphysics. In both cases, the fields are in excellent agreement with the verification case, reflecting the appropriate implementation of Eqs. 10 and 11. Similar levels of agreements are observed when the coil is replaced by a vertically magnetized magnet.

Figure 5 compares the magnetic force density for $I = 20$ A with Comsol Multiphysics. The distributions are practically identical both in module and direction, which verifies the correct implementation of the magnetic force formulations. Since the force depends on the spatial derivatives of the magnetic field, as reflected by Eq. (5c), it is highly sensitive to irregularities in $\boldsymbol{H}$ and $\boldsymbol{M}$. In the plot, slight instabilities are manifested as knots at the interface between domains A and D. However, they are much less significant than their Comsol Multiphysics counterpart, reflecting a robust implementation of the numerical method.

The implementation of the magnetic force term in the momentum balance is verified in Fig. 6. According to Eq. 9b, the steady state pressure lines must be coincident with the constant $\boldsymbol{H}$ lines for a linearly magnetized liquid. After implementing a constant magnetic susceptibility $\chi^{\text{vol}} = 0.1$, the comparison between both plots reflects the desired feature.

The shape of the meniscus is finally represented in Fig. 7 for the non-magnetic ($I = 0$ A) and magnetic ($I = 11$ A) cases and the physical properties reported in Ref. 29. The solution from a previous quasi-analytical magnetic sloshing model [33] is represented for comparison. Although the shapes are identical for the non-magnetic case, the magnetic result is slightly different. This may reflect fundamental differences between the physical models (e.g. level of fluid-magnetic coupling), the accumulation of numerical errors, or an error in the implementation. In order to understand this divergence and verify the computation of the meniscus, larger free surface deformations must be induced by simulating stronger magnets (see for instance Ref. [33]). However, strong magnetic fields require an excellent conditioning of the collocation matrices in region D, which is discretized by following a meshfree methodology. Small numerical errors give rise to the instabilities discussed in Fig. 5. Current efforts are consequently focused on the development of a robust and well-conditioned discretization for region D.

5 Conclusions

A fully coupled magnetohydrodynamic model has been developed to analyze the axisymmetric oscillations of magnetic liquids in microgravity. The model differs from previous works in the coupled
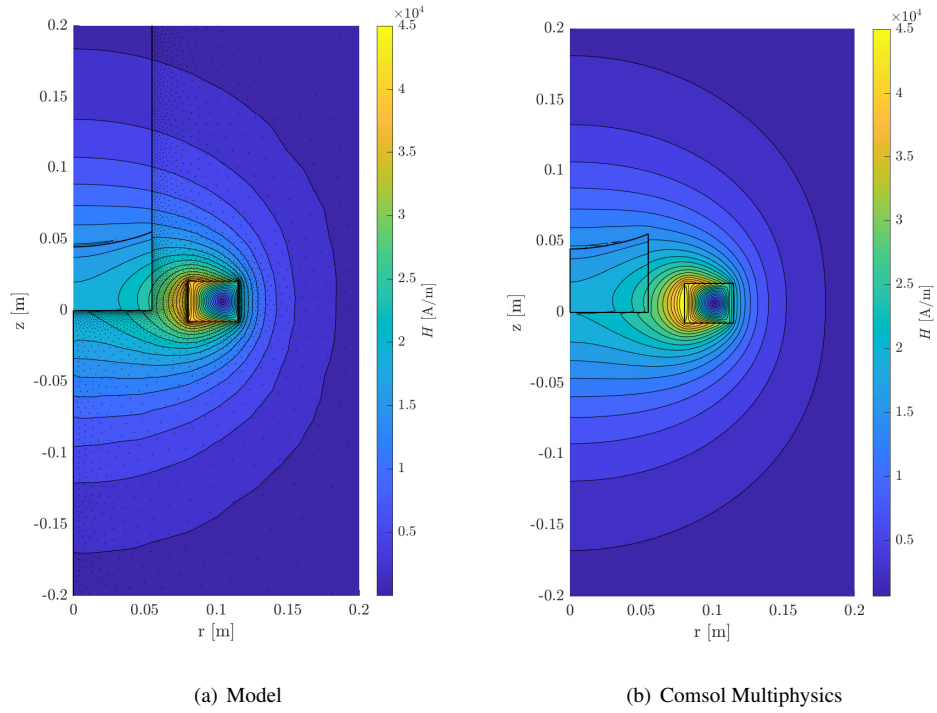
(a) Model

(b) Comsol Multiphysics

Fig. 3: Magnetic field comparison for $I = 20$ A.

(a) Model

(b) Comsol Multiphysics
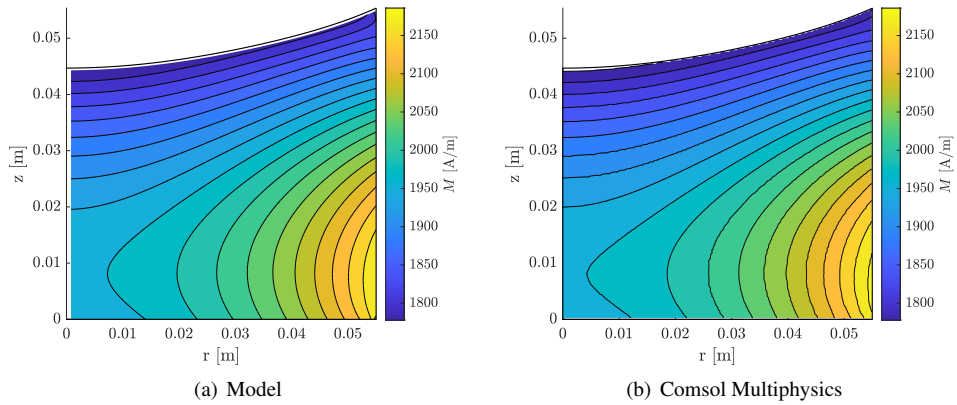
Fig. 4: Magnetization field comparison for $I = 20$ A.

(a) Model

(b) Comsol Multiphysics
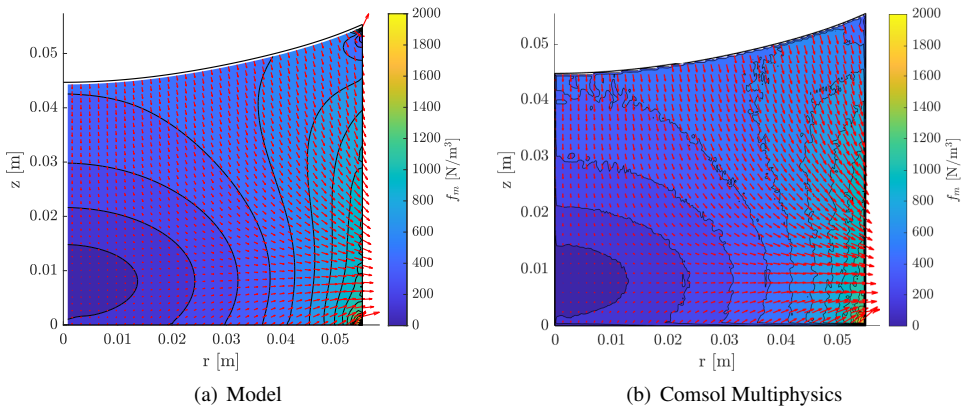
Fig. 5: Force density comparison for $I = 20$ A.
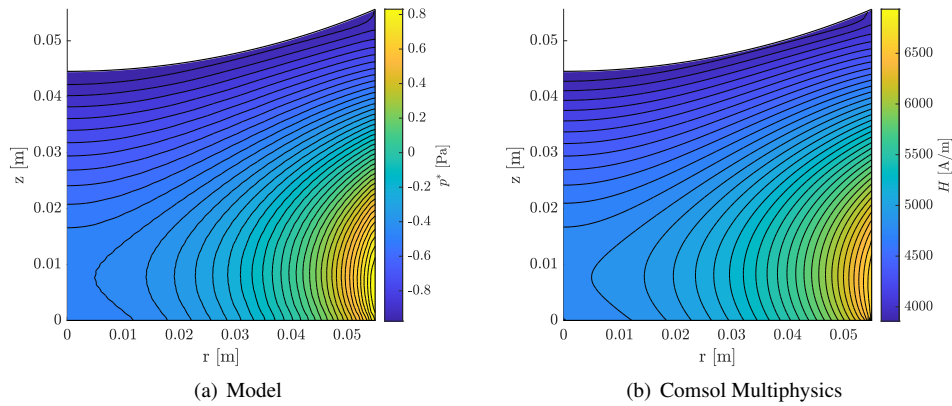
(a) Model

(b) Comsol Multiphysics

Fig. 6: Comparison of presssure and magnetic field lines for a paramagnetic fluid with $\chi^{\text{vol}} = 0.1$.

solution of the fluid-magnetic problem and the adoption of a highly efficient, monolithic, and implicit numerical approach. These key characteristics enable the analysis of highly susceptible magnetic liquids, such as ferrofluids.

The magnetic solution from the steady-state Maxwell equations has been verified with equivalent simulations in Comsol Multiphysics. The magnetic momentum balance has also been verified by comparing the steady-state magnetic field and pressure contours for a linearly magnetized liquid. The comparison of the meniscus profile with a previous quasi-analytic magnetic sloshing model has shown a virtually perfect agreement in the non-magnetic case. However, stronger magnetic fields (i.e. optimum conditioning of the meshless region D) are required to perform an accurate verification for the magnetic case.

Although the ESA Drop Your Thesis! 2017 configuration has been implemented to ease the verification of results, the numerical model here introduced finds application in many other scenarios of scientific and technical interest. Some of them involve the study of axisymmetric tank geometries, viscous liquids, magnetically-induced viscosity, free surface stability, or time-dependent simulations. Although significant efforts need to be carried out to extend this work to the 3D case (lateral sloshing) and improve the robustness of numerical computations, this already represents a promising step towards the development of future applications.
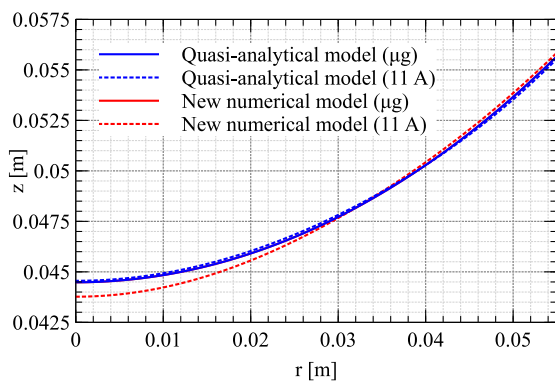

Fig. 7: Comparison of meniscus interfaces with a previous quasi-analytical model [33] for the non-magnetic and magnetic ($I = 11$ A) cases.

References

[1] M. Eswaran and U. K. Saha. "Sloshing of liquids in partially filled tanks - a review of experimental investigations". In: *Ocean Systems Engineering* 1.2 (2011), pp. 131–155.

[2] W. C. Reynolds and H. M. Satterlee. "Ch. 11 - Liquid Propellant Behavior at Low and Zero g". In: *The Dynamic Behavior of Liquids in Moving Containers*. NASA SP-106, 1966.

[3] F. Dodge. *The New Dynamic Behavior of Liquids in Moving Containers*. Southwest Research Institute, 2000. Chap. Ch. 4 - Fluid Management in Microgravity.

[4] A. Y. Lee and J. Stupik. "In-Flight Characterization of the Cassini Spacecraft Propellant Slosh Modes". In: *Journal of Spacecraft and Rockets* 54.2 (2017), pp. 417–425.

[5] D. Chipchark. "Development of expulsion and orientation systems for advanced liquid rocket propulsion systems". In: *USAF Technical Report RTD-TDR-63-1048, Contract AF04 (611)-8200* (1963).

[6] J. J. Martin and J. B. Holt. "Magnetically Actuated Propellant Orientation Experiment, Controlling fluid Motion With Magnetic Fields in a Low-Gravity Environment". In: *NASA/TM-2000-210129, M-975, NAS 1.15:210129* (2000). Ed. by NASA.

[7] S. Papell. "Low viscosity magnetic fluid obtained by the colloidal suspension of magnetic particles". In: *US Patent 3215572* (1963).

[8] Á. Romero-Calvo, F. Maggi, and H. Schaub. "Prospects and challenges for magnetic propellant positioning in low-gravity". In: *Proceedings of the AAS Guidance, Navigation and Control Conference, Breckenridge, Colorado*. 2020, pp. 497–515.

[9] S. Kaneko, T. Ishiyama, and T. Sawada. "Effect of an applied magnetic field on sloshing pressure in a magnetic fluid". In: *Journal of Physics: Conference Series* 412.1 (2013), pp. 012–018.

[10] M. Ohaba and S. Sudo. "Liquid surface behavior of a magnetic liquid in a container subjected to magnetic field and vertical vibration". In: *Journal of Magnetism and Magnetic Material* 149 (1995), pp. 38–41.

[11] S. Sudo, H. Nishiyama, K. Katagiri, and J. Tani. "Interactions of Magnetic Field and the Magnetic Fluid Surface". In: *Journal of Intelligent Material Systems and Structures* 10.6 (1999), pp. 498–504.

[12] T. Ishiyama, S. Kaneko, S. Takemoto, and T. Sawada. "Relation between Dynamic Pressure and Displacement of Free Surface in Two-Layer Sloshing between a Magnetic Fluid and Silicone Oil". In: *Materials Science Forum* 792 (June 2014), pp. 33–38.

[13] T. Sawada, Y. Ohira, and H. Houda. "Sloshing motion of a magnetic fluid in a cylindrical container due to horizontal oscillation". English. In: *Energy Conversion and Management* 43.3 (2002), pp. 299–308.

[14] K. Ohno, M. Shimoda, and T. Sawada. "Optimal design of a tuned liquid damper using a magnetic fluid with one electromagnet". In: *Journal of Physics: Condensed Matter* 20.20 (2008), p. 204146.

[15] K. Ohno, H. Suzuki, and T. Sawada. "Analysis of liquid sloshing of a tuned magnetic fluid damper for single and co-axial cylindrical containers". In: *Journal of Magnetism and Magnetic Materials* 323.10 (2011). Proceedings of 12th International Conference on Magnetic Fluid, Sendai, Japan, pp. 1389–1393.

[16] F. T. Dodge and L. R. Garza. "Free-Surface Vibrations of a Magnetic Liquid". In: *Journal of Engineering for Industry* 94.1 (1972), pp. 103–108.

[17] J. Hochstein, J. R. Warren, J. George Schmidt, J. Hochstein, J. R. Warren, and J. George Schmidt. "Magnetically Actuated Propellant Orientation (MAPO) Experiment - Pre-flight flow field predictions". In: *35th Aerospace Sciences Meeting and Exhibit*. 1997.

[18] J. G. Marchetta and J. Hochstein. "Fluid capture by a permanent ring magnet in reduced gravity". In: *Proceedings of the 37th Aerospace Sciences Meeting and Exhibit, Reno, NV, USA*. American Institute of Aeronautics and Astronautics, 1999.

[19] J. G. Marchetta and J. Hochstein. "Simulation and dimensionless modeling of magnetically induced reorientation". In: *Proceedings of the 38th Aerospace Sciences Meeting and Exhibit, Renno, NV, USA*. American Institute of Aeronautics and Astronautics, 2000.

[20] J. G. Marchetta, J. Hochstein, D. Sauter, and B. Simmons. "Modeling and prediction of magnetic storage and reorientation of LOX in reduced gravity". In: *40th AIAA Aerospace Sciences Meeting & Exhibit*. American Institute of Aeronautics and Astronautics, 2002. Chap. AIAA Paper 2002-1005.

[21] J. G. Marchetta. "Simulation of LOX reorientation using magnetic positive positioning". In: *Microgravity - Science and Technology* 18.1 (Mar. 2006), pp. 31–39.

[22] J. G. Marchetta and K. Roos. "A Three-Dimensional Computational Simulation of Magnetic Positive Positioning". In: *45th AIAA Aerospace Sciences Meeting and Exhibit, Reno, Nevada*. 2007. Chap. AIAA Paper 2007-956.

[23] J. G. Marchetta and K. Roos. "Simulating Magnetic Positive Positioning of Liquids in a Transient Acceleration Field". In: *46th AIAA Aerospace Sciences Meeting and Exhibit, Reno, Nevada*. 2008. Chap. AIAA Paper 2008-820.

[24] J. G. Marchetta, B. D. Simmons, and J. I. Hochstein. "Magnetic retention of LO2 in an accelerating environment". In: *Acta Astronautica* 62.8 (2008), pp. 478–490.

[25] J. G. Marchetta and A. P. Winter. "Simulation of magnetic positive positioning for space based fluid management systems". In: *Mathematical and Computer Modelling* 51.9 (2010), pp. 1202–1212.

[26] Á. Romero-Calvo, T. H. Hermans, G. C. Gómez, L. P. Benítez, M. H. Gutiérrez, and E. Castro-Hernández. "Ferrofluid Dynamics in Microgravity Conditions". In: *Proceedings of the 2nd Symposion on Space Educational Activities, Budapest, Hungary*. 2018.

[27] Á. Romero-Calvo, T. H. Hermans, L. P. Benítez, and E. Castro-Hernández. *Drop Your Thesis! 2017 Experiment Report - Ferrofluids Dynamics in Microgravity Conditions*. European Space Agency - Erasmus Experiment Archive, 2018.

[28] Á. Romero-Calvo, G. Cano-Gómez, T. H. Hermans, L. Parrilla Benítez, M. Herrada Gutiérrez, and E. Castro-Hernández. "Total magnetic force on a ferrofluid droplet in microgravity". In: *Experimental Thermal and Fluid Science* 117 (2020), pp. 110–124.

[29] Á. Romero-Calvo, M. Á. Herrada, T. H. Hermans, L. P. Benítez, G. Cano-Gómez, and E. Castro-Hernández. "Axisymmetric ferrofluid oscillations in a cylindrical tank in microgravity". In: *Journal of Applied Mechanics, under review.* (2020).

[30] Á. Romero-Calvo, A. García-Salcedo, F. Garrone, I. Rivoalen, G. Cano-Gómez, E. Castro-Hernández, M. H. Gutiérrez, and F. Maggi. "StELIUM: A student experiment to investigate the sloshing of magnetic liquids in microgravity". In: *Acta Astronautica* 173 (2020), pp. 344–355.

[31] Á. Romero-Calvo, A. García-Salcedo, F. Garrone, I. Rivoalen, G. C. Gomez, E. Castro-Hernández, and F. Maggi. "Free Surface Reconstruction of Opaque Liquids for Experimental Sloshing Analyses in Microgravity". In: *Proceedings of the 70th International Astronautical Congress, Washington DC, USA*. 2019.

[32] M. Herrada and J. Montanero. "A numerical method to study the dynamics of capillary fluid systems". In: *Journal of Computational Physics* 306 (2016), pp. 137–147.

[33] Á. Romero-Calvo, G. Cano Gómez, E. Castro-Hernández, and F. Maggi. "Free and Forced Oscillations of Magnetic Liquids Under Low-Gravity Conditions". In: *Journal of Applied Mechanics* 87.2 (2020). 021010.

[34] L. Landau and E. Lifshitz. *Electrodynamics of Continuous Media*. Pergamon Press, 1960.

[35] A. Engel and R. Friedrichs. "On the electromagnetic force on a polarizable body". In: *American Journal of Physics* 70.4 (2002), pp. 428–432.

[36] R. E. Rosensweig. "Continuum equations for magnetic and dielectric fluids with internal rotations". In: *The Journal of Chemical Physics* 121.3 (2004), pp. 1228–1242.

[37] R. E. Rosensweig. "Stress Boundary-Conditions in Ferrohydrodynamics". In: *Industrial & Engineering Chemistry Research* 46.19 (2007), pp. 6113–6117.

[38] R. E. Rosensweig. *Ferrohydrodynamics*. Dover Publications, 1997. ISBN: 9780486678344.

[39] M. Shliomis. "Effective Viscosity of Magnetic Suspensions". In: *Soviet Physics JETP* 34 (1972), pp. 1291–1294.

[40] D. Engwirda. "Locally optimal Delaunay-refinement and optimisation-based mesh generation". Doctor of Philosophy Ph.D. University of Sydney; Faculty of Science; School of Mathematics and Statistics, 2014.

[41] G. Liu. *Mesh Free Methods: Moving Beyond the Finite Element Method*. CRC Press, 2002. ISBN: 9781420040586.